ARTICLE

Application of AI Enhanced Digital Terrain Classification and Automatic Micro Terrain Extraction in Power Line Engineering

Rui He[1,*], Xin Wan[1], Binbin Xu[1], Tianyou Yan[1] and Xiaoying Chen[1]

[1] Guangzhou Power Supply Bureau Project Management Center, Guangdong Power Grid Co., Ltd., Guangzhou 510062, Guangdong

Abstract

Accurate terrain classification and micro terrain extraction are of great significance for line planning, equipment layout, and inspection and maintenance in power line engineering. However, due to the complex terrain traversed by transmission lines, traditional extraction methods face challenges in dealing with large-scale point cloud data and irregular terrain. This article develops a method of digital terrain classification and automatic extraction of micro-terrain through AI enhancement to resolve the present problems of high computational complexity, accumulation of errors, and limited accuracy in ground point extraction. This technique combines the CNN and progressive triangulation algorithms to optimally improve the construction of triangulation networks by making an intelligent prediction of the trends of terrain change. In addition, this paper developed an automated micro terrain extraction system that can robustly identify key terrain features along transmission lines in complex backgrounds. Experimental results have demonstrated that the proposed method outperforms traditional methods on large-scale point cloud data and is suitable for practical applications in power line engineering.

Keywords: artificial intelligence enhancement, digital terrain classification, transmission line engineering, point cloud data, progressive triangular network algorithm

Submitted: 16 August, 2024
Accepted: 30 November, 2024
Published: 19 December, 2024

Vol. 2024, **No.** 1, 2024.

***Corresponding author:**
✉ Rui He
herui522@163.com

Citation
Rui He, Xin Wan, Binbin Xu, Tianyou Yan and Xiaoying Chen (2024). Application of AI Enhanced Digital Terrain Classification and Automatic Micro Terrain Extraction in Power Line Engineering . Mari Papel Y Corrugado, 2024(1), 132–142.

1 Introduction

Recently, with the demand for power line inspections, this remote sensing technology based on drones has been extensively used to obtain large-scale point cloud data along transmission lines [1]. The large amounts of terrain information in the point cloud data offer a basis for achieving high-precision terrain classification and micro terrain extraction [2]. However, due to the large scale of data and complex terrain, how to accurately and quickly extract ground points and key terrain features from it has become one of the current research hotspots [3]. Traditional ground point extraction methods, such as those based on Irregular Triangular Networks (TINs), can capture detailed features of the terrain to a certain extent. Nevertheless, because static construction of network is flawed, cumulative error is very easy to have the tendency, especially in terrain conditions [4].

In terms of power line engineering, microterrain is of great significance, which exerts important effects on construction plan, arrangement, and monitoring and maintenance in engineering, and can reflect the conditions of a site [5]. Although typical transmission lines cross complicated mountain terrain or terrains, hills, river valley, etc., the original approach, such as terrain classification plus direct and extraction of ground points, face difficulties in dealing with complicated irregular terrain, which could lead to low

efficiency of the algorithm, error accumulation, and difficulty in large-scale point cloud data, etc. Therefore, on the basis of progressive triangulation, ground point-extracting algorithms have begun to attract attention gradually [6]. This algorithm will update and adjust the structure of the triangular network while efficiently reducing the accumulation of errors during the process of updating it in order to improve accuracy over terrain extraction [7]. Nevertheless, while good performance is observed over smaller-scale point cloud data, high computational complexity and memory storage bottlenecks exist regarding large-scale point cloud data processing during power line inspection.

The point cloud data obtained in the power line patrol process is usually of a large scale, and the distribution of point clouds along the line direction presents irregular stripes [8]. The traditional grid partitioning method often generates a large number of redundant grids or leads to extraction errors when processing such data [9]. Usually, transmission lines tend to pass through mountainous river valley areas where the terrain is largely variant and poses serious challenges in terms of precise extraction of ground points [10]. It proves hard for traditional algorithms dealing with such complex terrains in an effective manner whereby significant key ground points would easily be omitted or miscorrected [11]. The progressive triangulation-based ground point extraction algorithm does indeed improve accuracy, but at a high computational complexity that exponentially grows with an increase in the volume of point cloud data, hence becoming difficult to achieve fast processing on large datasets [12]. In the process of terrain classification and micro terrain extraction, the presence of target structures such as power lines and transmission towers, as well as interference from backgrounds such as trees and buildings, increase the difficulty of the extraction algorithm [13]. How to extract effective ground information in complex backgrounds is an urgent problem to be solved.

The current research mainly focuses on how to improve the accuracy and efficiency of terrain classification and ground point extraction. The algorithms based on irregular triangulation and progressive triangulation are currently two commonly used methods [14]. Among them, although the Irregular Triangular Network (TIN) method is computationally simple, it is prone to error accumulation due to the limitations of static network construction [15]. As stated by the authors, progressive triangulated irregular network algorithm resolves errors when such accumulation occurs by adapting at each level by changing the structure of a triangulation network; performance is good in continuous-terrain extraction [16]. However, the progressive algorithm for triangulation suffers the drawback of high computational cost, especially when applied for large-scale point cloud, and the efficiency of application is low. Additionally, the algorithm still lacks appropriate extraction accuracy when handling with complex terrain.

Existing methods for data processing in the process of power line inspection are based primarily on techniques of traditional image processing and point cloud analysis. These can satisfy some engineering requirements but lack support from intelligent algorithms and have poor performances in handling complex scenarios and large-scale data [19]. Especially in the field of automated micro terrain extraction, the methods available so far mostly rely on manual intervention and are unable to achieve full automation and intelligence. This article therefore explores digital terrain classification and automatic micro-terrain extraction based on the enhancement of artificial intelligence and proposes an algorithm framework for accurate extraction of key ground points and micro-terrain features in complex terrain environments combined with specific needs in power line engineering.

2 Ground Point Extraction Algorithm Based on Progressive Triangulation

2.1 Principle of ground point extraction algorithm based on progressive triangular network

The ground point extraction algorithm based on progressive triangulation is an improvement that combines the irregular triangulation algorithm with the progressive triangulation algorithm. Compared with the ground point extraction method based on irregular triangulation, the algorithm based on progressive triangulation can readjust the ground triangulation based on the extracted ground points, thus solving the cumulative error of ground point extraction caused by static network construction in the irregular triangulation algorithm.

The main process of ground point extraction based on progressive triangulation is as follows: (1) Ground seed point extraction; (2) Construct an initial triangulation network (TIN) based on the extracted ground seed points; (3) Extract ground points based on the initial triangulation and construct a progressive

triangulation.

2.2 Ground point extraction algorithm based on progressive triangular network

The process of ground point extraction based on progressive triangulation is divided into: (1) ground seed point extraction; (2) Construct an initial triangular network based on the extracted ground seed points; (3) Extract ground points and construct a progressive triangulation based on the initial triangulation. Compared with other datasets, the dataset obtained during the power line patrol process has its own characteristics, so there are some differences in the extraction process used. Analyze the main process of the ground point extraction algorithm based on progressive triangulation in the power line patrol process.

2.3 Extraction of ground seed points

In power applications, point cloud data is usually acquired along transmission lines, so the data will appear in stripes as shown in Figure 1:

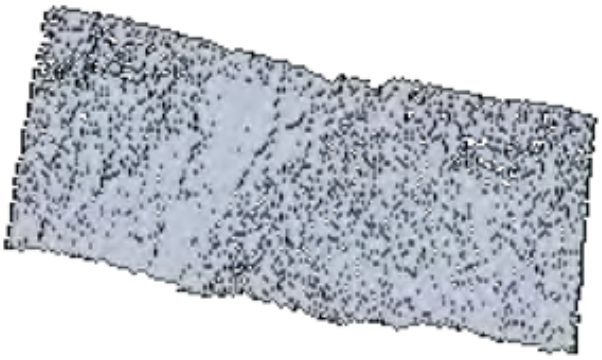

Figure 1. Distribution of patrol point cloud

If traditional methods are used for grid partitioning, there will be a large number of redundant grids that do not contain any laser points, or grids that contain less data, resulting in extraction errors. To reduce the calculation error caused by irregular strip lines, this paper adopts the method of grid division along the line direction to improve the accuracy of key ground point extraction, as shown in Figure 2:

The grid size used needs to be larger than the size of the buildings to ensure that the effects of the building surfaces do not impact the key points on the ground. In contrast, a grid too large would lead to all the points at the top of the mountain being filtered out and hence errors. Accordingly, for ground point extraction in general, the maximum one-size grid of any largest single building is utilized. Profile of extracted point ground cloud is given by the Figure 3

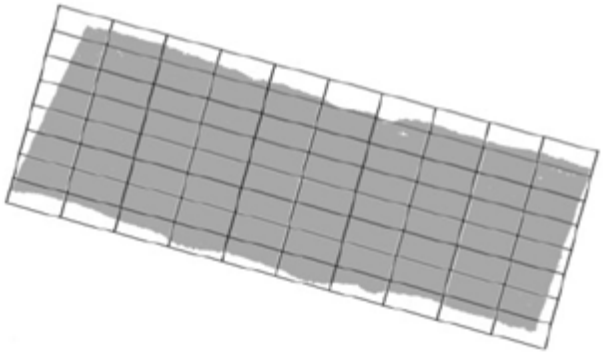

Figure 2. Grid division along the direction of point cloud distribution

Figure 3. Side view of Ground grid point extraction

Figure 3 Side view of grid point extraction Figure 4 Front view of ground grid points From Figure 3, it can be found that the method for extracting the lowest point of the grid can effectively extract the ground seed points.

Figure 4. Front view of ground grid points

2.3.1 *Construction of irregular triangular network*

Based on the extracted grid points, an irregular triangular network is constructed as shown in Figure 5:

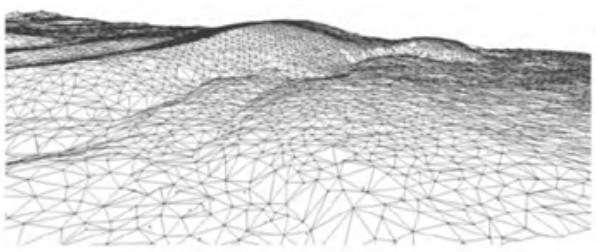

Figure 5. Construction of surface point triangulation network

Figure 5 shows the local area of the ground triangulation network constructed based on extracting ground points. Generally speaking, the construction

of triangulation is carried out using Delaunay triangulation. The two main principles of Delaunay triangulation are: (1) The hollow circle criterion, which means that the circumcircle of the triangle formed does not contain the fourth point; (2) Maximizing the minimum angle criterion, selecting the construction method of the triangular network with the minimum angle and the maximum angle among the triangular networks that meet the conditions.

The implementation methods of Delaunay triangulation mainly include point by point insertion method, triangulation growth method, and divide and conquer method. Although using the split method has high efficiency, in the application of power line patrol, due to the huge amount of point cloud data and the need for continuous adjustment of the constructed triangulation network, the point by point insertion method is chosen to triangulate the extracted ground seed points.

2.3.2 *Progressive triangular network construction*

The progressive triangulation construction method is as follows:

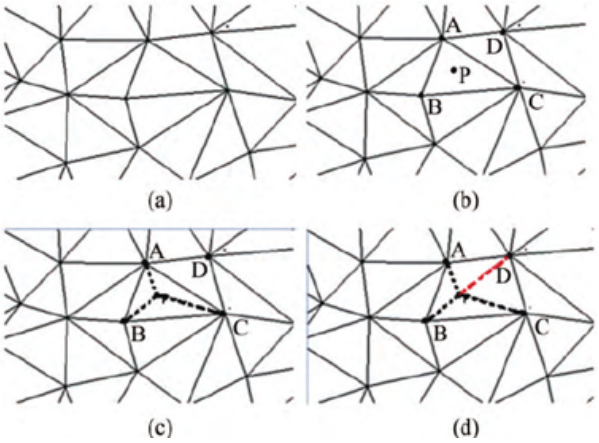

Figure 6. Ground point extraction of progressive triangulation network

The ground point extraction process flow based on progressive triangulation is presented in Figure 6. In Figure 6, the Figure 6(a) illustrates a locally enlarged view of the ground point triangulation. As shown in Figure 6(b) is the point that is to be computed. Compute which triangle network the point P belongs to. Let the triangle that needs to be determined be triangle ABC. The procedure to calculate which point in the triangle network is as follows:

$$\overrightarrow{AP} = u\overrightarrow{AB} + v\overrightarrow{AC}. \quad (1)$$

Since ABC can form a triangle, any vector in space can be linearly represented by vectors $\overrightarrow{AB}$ and $\overrightarrow{AC}$, with u and v as coefficients. If point P is in triangle ABC, u and v need to satisfy the following conditions:

$$1 \geq u \geq 0, \quad (2)$$

$$1 \geq v \geq 0, \quad (3)$$

$$u + v \leq 1. \quad (4)$$

According to Eqs. (1) to (4), the triangle where point P is located can be determined. If P is located in the triangle formed by point ABC, the distance between point P and the face formed by triangle ABC, as well as the minimum angle between the three vertices of point P and triangle ABC and face ABC, can be determined.

The distance from point P to surface ABC is:

$$d = \frac{|aX_p + bY_p + cZ_p + d|}{\sqrt[2]{a^2 + b^2 + c^2}}. \quad (5)$$

The angle between point P and ABC is:

$$\alpha_i = \arcsin\left(\frac{d}{dP_i}\right). \quad (6)$$

In the formula, d is the distance from P to surface ABC.

$$dP_i = \sqrt[2]{(X_p - X_i)^2 + (Y_p - Y_i)^2 + (Z_p - Z_i)^2}. \quad (7)$$

In the formula, $i = A, B, C$. If the distance and minimum angle are both less than the threshold, point P is considered a ground point. Then, point P is added to the ground point triangulation and the triangulation is readjusted to form a new triangulation as shown in Figure 6(d). For all point cloud data, perform the above steps until there are no newly added point clouds in the triangulation, and then all point clouds used to construct the triangulation are ground points.

3 Power Cord Testing

Another difficult challenge is identifying electrical lines (ropes) from aerial pictures because of the cluttered background. The edge map is significantly noisy due to fields, trees, shrubs, and mountains (Figure 7a). Furthermore, the edge equivalent of power lines is not a straight line because of the natural sagging of power lines (Figure 7b). As a result, there will eventually be a lot of false positives from the power line detection approach employing Hough lines. Nevertheless, because of the drone's flying posture,

these power cords are visible in the inspection video as components that are linked horizontally to the camera. As a result, this paper suggests using a specially designed kernel to calculate edge mappings (Figure 7c). Algorithm 1 provides an algorithm for detecting power lines.

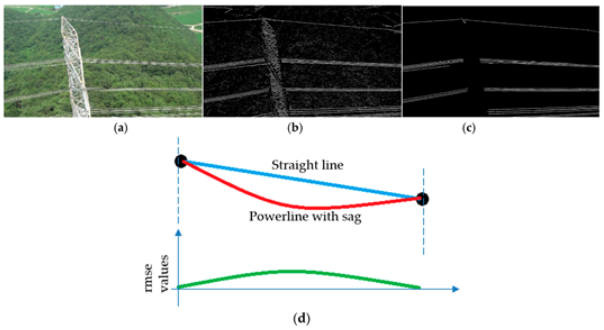

Figure 7. (a) shows the transmission tower and power line from above. (b) Edge counterparts are extremely loud because of the trees and numerous items in the background. (c) Using custom shaped Sobel kernels can help eliminate noise. (d) Connect the imaginary straight blue line with concave power lines (red) at their endpoints. The root mean square error (RMSE) value between the line and the power function is shown on the green curve

To obtain the edge map, first convert the input image to grayscale. Next, convolve the customized kernel with the grayscale image. To get rid of weak and noisy edges, threshold the edge map. Next, apply connected component analysis to remove edges with lengths less than the specified threshold ($th_{edgelength}$) and edges that appear vertically in the edge graph, because there is extremely little chance that these edges will join the electrical line. Determine the endpoints of the remaining edges, then use the two edge endpoints to compute the line's equation. Next, calculate the root mean square error (RMSE) between all points on the line and edge. Finally, if the RMSE value is less than the specified threshold, the algorithm selects the edge as the valid power line (th_{rmse}).

The natural indentation in the power line leads to an increase in RMSE value, resulting in a low recall rate of the power line. Therefore, another parameter called edge curvature is introduced. The depression of the power line always occurs downwards, causing the curved edge to bend upwards (Figure 7d). As a result, the suggested power line detection algorithm determines the final edge's curvature and confirms that it is upward.

As demonstrated in Figure 8, the suggested power line detection method may produce good detection results even in cluttered backdrops, dim lighting, and power line depressions.

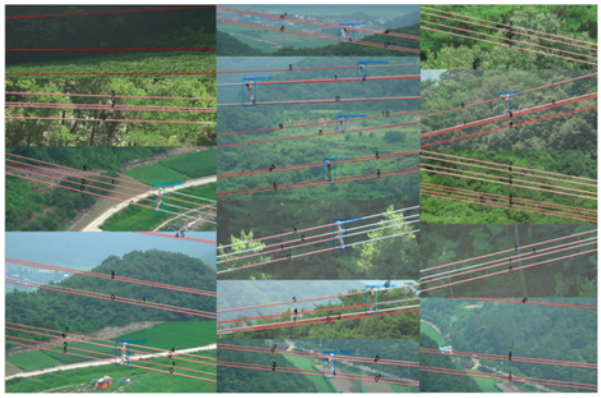

Figure 8. Power cord test findings. The suggested approach for detecting electricity lines is resilient to various lighting conditions and crowded backdrops. An ID number is written on the red-marked power cord that has been detected

4 Defect Analyzer

The technique for identifying transmission line components from real-time drone videos was presented in the preceding section. The defect analyzer will receive the cropped photos of the components when they have been identified. Poor design, careless manufacturing, using inferior materials during the manufacturing process, incorrect insulator use, extreme mechanical forces related to weather (rain, storms, snow, hail, humidity, extreme cold and hot temperatures, and UV radiation), intentional destruction, wildlife, extreme electrical activities, or improper handling can all result in defects in high-voltage transmission line components.These flaws can cause electrical components to change color (from flashover and extremely hot temperatures, for example), shape (from cracks, holes, and broken lids, for example), and/or texture (from breakage, fragmentation, cracks, etc.). A qualitative indicator of the degree to which particular kinds of transmission line components are close to failing is provided by the suggested defect analyzer.

Seven distinct transmission types' deformation defect circuit components can be found using the suggested defect analyzer. The suggested flaw detection algorithm is explained in the section that follows.

4.1 PorSTI-W and PorSTI-R shed or disk breaks

In each type of insulator shown in Figures 9b-d, the repeated circular portions are referred to as "sheds" or "caps". Small fissures on the ceramic disc's surface, brought on by thermal stress or uneven heating, are

the source of the fracture and detachment flaws in PorSTI-W and PorSTI-R. These fissures will enlarge with time due to mechanical tension and severe winds, ultimately resulting in the complete fracture of a single disc, as illustrated in Figure 9a.

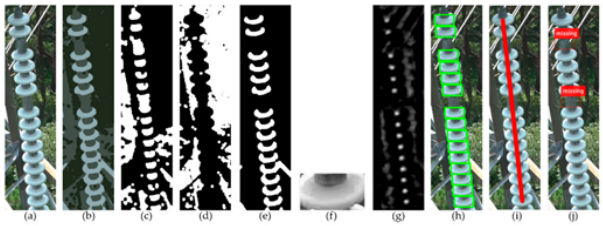

Figure 9. How to identify damage to a shed. (a) Identifying insulator images using CNN-based detectors; (b) segmentation outputs using color clustering; (c–e) segmentation masks for three clusters; (f) candidate templates and connected component analysis following maximum voting to identify the most recurring patterns; (g) activation maps matched by templates; (h) template matching outcomes; (i) fitting the centers of template matching outcomes into straight lines; and (j) final defects detected

The visual symmetry and spatial contextual information of the insulator shape were used to identify broken or absent ceramic disks in the cropped insulator image. The suggested technique uses example templates of ceramic sheds that are obtained from input insulation photos to iteratively search for missing sheds because of the emergence of equidistant repeated patterns in the insulation shed. Figure 9 displays the missing shed/disk detection algorithm.

The approach for sample templates is to first build color clusters on the input image (Figure 9b), then apply morphological operations to discover suitable template areas, and then refine them using contextual priors (Figures **??**c – e illustrate three refined clusters). To acquire statistical information on the shape of spots within the clusters, use connected component analysis to three refined clusters. The cluster with the greatest proportion of evenly spaced and sized spots (Figure 9e in this example) is chosen by the algorithm. Then, each template proposal is convolved with the input insulator picture in a sliding window fashion after being extracted from the chosen cluster (Figure 9f). Finally, the greatest response region (Figure 9g) is clustered (Figure 9h).Subsequently, the algorithm determines the fitting error and fits the largest response area as a straight line (Figure 9i). The algorithm rejects the proposal and the maximum response as false positives if the fitting error exceeds the predetermined threshold (set on the validation dataset). If the fitting error is less than the predetermined threshold, the maximum response is regarded by the algorithm as the detected insulator detachment/disk. Next, the algorithm splits the data into two groups based on the paired distances between the shed/disc centers. Smaller groupings are referred to as outliers, and missing or broken sheds/disks are indicated in the space between pairs of outliers (Figure 9j).

4.2 Respondent's flaw of color fading

A colored, spherical transmission line component attached to a transmission line is called a responder, sometimes referred to as a responder beacon. Responders are used to visually alert low-flying objects of their presence in order to avoid collisions. Their bright coatings may peel off due to prolonged use, dust, high winds, and rain, which would reduce their visibility and may endanger things that are flying at low altitudes.

The spherical responder body is initially clipped from the detection data in order to find fading faults in the responder. The responder image is degraded to lower the color variation range of the background and foreground (responder subject) in order to mask the noisy background (Figure 10b). Considering that the respondent's image is mostly made up of three color clusters: the background, the respondent's top (brighter than lower) portion, and the respondent's bottom portion. This supposition leads to the division of the image into three color clusters (Figure 10c), which are chosen as the foreground and show a high likelihood of recall values in the image's center (Figure 10d).Figure 10e illustrates how the foreground is suppressed. A Gaussian Laplacian (LoG) filter is then applied to identify areas with abrupt changes in intensity. As seen in Figures 10f–h, this filter is applied to the red and saturation color spaces since they are the most discriminative in identifying responder flaws. As seen in Figure 10l, highlight the problematic locations after eliminating background noise and boundary regions.

4.3 Splitting and breakdown detection of polymer insulators

Polymer insulators can develop cracks for a number of causes, such as poor manufacturing quality materials or procedures, improper handling during installation or shipping, deliberate damage, birds, etc. Any of these scenarios will cause cracks to spread radially in the direction of the insulator's core, exposing the metal rod and perhaps endangering nearby electrical infrastructure.

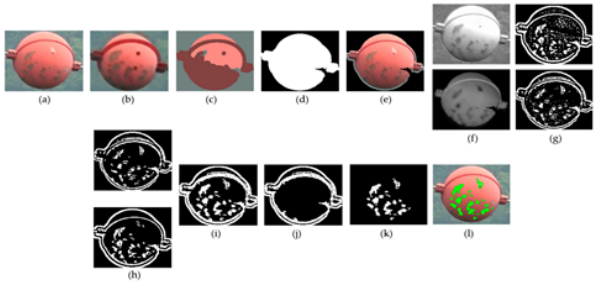

Figure 10. Procedures for identifying respondent flaws. (a) CNN is used to detect the input image; (b) color clustering is applied; (c) after erosion; (d) foreground mask is applied following clustering selection and region filling; (e) mask foreground; (f) responder images in red and saturated color spaces are filtered; (h) noise is removed from (g); (i) red and saturated space outputs are combined in (h); and (j) mask is applied in boundary regions

Owing to the insulator cap's elliptical shape, it is advised to separate the cap using the ellipse detection technique before applying the split detection algorithm to each individual cap.The segmentation detection algorithm begins with the insulator picture's rotation normalization since the ellipse detection technique assumes that the insulator image is rotation normalized. Figure 11 displays the findings of certain cap detection using the author's ellipse detector (after rotation normalization).

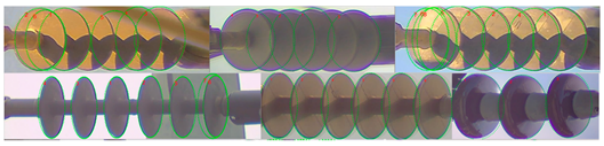

Figure 11. Results of elliptical detection for various insulator kinds. Red highlights the ellipse with the highest confidence level, which is numbered in ascending order

The algorithm uses the identified ellipses to protect the insulator's cover while applying the crack detection algorithm to a single cover. The boundary of the cap is subtracted from its edge map by the segmentation detection algorithm after it has first computed the edge map of the cap. The program then goes through each edge inside the lid one by one. The contour is closed and the area of the closed contour is computed if the edge is near the lid's boundary. The edge is handled as noise otherwise. Figure 12 illustrates the split detection algorithm's processes.

5 Results and Discussion of the Experiment

The transmission line component detection system's experimental findings are presented in this section.

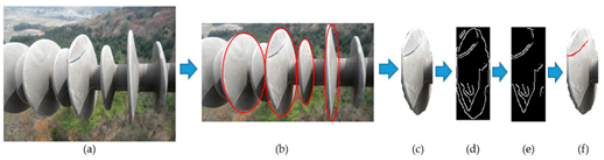

Figure 12. Polymer insulators' crack detecting procedure. A) The input picture; B) the result of the ellipse detection; C) one of the segmentation caps; D) the edge map; E) the edge map following boundary removal; and F) the segmentation detection result

5.1 Database gathering

Only a few studies have used self-obtained databases to objectively evaluate system performance; currently, there is no publicly available dataset of transmission line images. A sizable unconstrained transmission line inspection video dataset that was shot using drones was gathered for the experiment described in this article. Drones are utilized to fly alongside transmission lines and towers, encompassing different kinds of transmission line components like insulators on transmission towers, damping counterweights, gaskets, responders, and sag adjusters.Furthermore, this article recommends the detection of transmission towers and power wires for future drone autonomous navigation. A total of 43 videos were captured, with an average of 700 frames. 30 videos in the training set, 10 videos in the testing set, and 3 videos in the validation set were all annotated.These movies were shot in two different lighting conditions—cloudy and sunny—between 11 a.m. and 3 p.m. The dataset, in the author's opinion, is impartial, unrestricted, and sizable enough to verify the dependability and efficiency of the suggested approach.

5.2 Inspection of components

It is limited to comparing the reported results with state-of-the-art approaches due to the absence of publicly available datasets. Only a small amount of research has been published that introduces the power line insulators' detection performance using the Pascal score—the same standard measurement that is employed in this article.

The suggested transmission line component detector's performance is assessed using the well-known Pascal score. The Pascal score is obtained by taking the intersection point (IoU) between the detected bounding $box \times BB_{detected}$ and the ground truth

bounding $box \times BB_{gt}$ as:

$$IoU = P(BB_{detected}, BB_{gt}) = \frac{Area(BB_{detected} \cap BB_{gt})}{Area(BB_{detected} \cup BB_{gt})}. \quad (8)$$

Table 1 displays the findings from the CNN-based transmission line component detector in two different configurations: (1) with YOLO V3 and (2) with multi-scale removed (strongly advised).

The statistical information from the training and testing datasets utilized to train the CNN-based transmission line component detector is also listed in Table 1. Table 1 also makes it abundantly evident that the CNN-based transmission line component detector is resilient to drastic alterations in scale and shape. The transmission tower, which may be seen in a variety of scales and orientations, is the most challenging object in our dataset.However, for transmission tower classes, CNN-based detectors show respectable detection performance. Furthermore, even with a limited quantity of training samples, CNN-based detectors demonstrate flawless detection outcomes for responder classes.

Table 1's performance comparison further suggests that eliminating multi-scale from YOLO V3 can enhance detection performance as a whole.Since the system is able to reject more false positives of cluttered items and its training concentrates more on detecting these objects at a single scale, accuracy and recall have significantly improved in the case of smaller components.e.

A comparison of published studies and the suggested transmission line component detection method is presented in Table 2. Direct comparisons are not possible due to differences in the assessment datasets between each study indicated in Table 2 regarding the number of test samples, picture resolution, and evaluation criteria. Comparisons, however, show that in comparable investigations, the suggested CNN-based embedded detector performs the best. The area under the precision recall curve, or average precision under various recall values, is what is meant to be understood when we talk about 'average precision' in Table 2.

5.3 Power cord testing

By analyzing detection time and accuracy on the gathered dataset, the suggested power line detection approach was contrasted with similar research. The comparison employed the implementations of EDLines and LSD. Three movies of power line inspection were annotated for evaluation purposes. Draw a line two pixels wide linking the power line's ends in the frame in question for each power line, and then save the binary mask of the annotated image as the ground truth value.

Determining the point of intersection between the detected line and the ground truth line is one of the evaluation criteria.The line is deemed true if the overlap is greater than 50%. In contrast to Pascal score, which is determined by utilizing the area of bounding boxes, in this case the area of lines is determined by their pixel count. Determine which pixels on the detection line are collinear with the ground truth line in order to compute the overlap. The performance comparison between the suggested power line detection method and two recent similar techniques is shown in Table 3. It is clear that in terms of accuracy and detection speed, the suggested power line detector works better than cutting-edge techniques.

One of the reasons why EDLines and LSD displayed poor power line recognition results on this dataset is that due to the natural sagging of power lines, they do not seem straight but rather somewhat bent. Consequently, they were eventually identified as several straight lines by EDLines and LSD, yielding a precision recall curve in Figure 13 that shows a high recall but low accuracy. The suggested method performs better than the state-of-the-art scheme because it accounts for the power line's natural sag. on assess the detection speed, EDLines, LSD, and the new approach were applied on a 1920 x 1080 image. Because the suggested algorithm employs a bespoke Sobel filter, which yields comparatively clean edge maps in contrast to EDLines and LSD, it is also the fastest of the three techniques. Furthermore, the suggested algorithm's search space is further reduced by the noise removal stage.The effectiveness of three approaches for power line detection is displayed in Figure 14. The decline is modest because LSD (first line: Figure 14) generates more false positives. Because EDLines (Figure 14) have a stronger ability to remove noise edges than LSD, it performs better than LSD. On the transmission tower, EDLines also produced a lot of false alerts in contrast to the suggested fix (second row, second column, Figure 14).

5.4 Defect analysis

The challenge of gathering a substantial number of photos of defective components is one of the

Type of Components	YOLO V3					YOLO V3 (Without Multi-Scaling)	
	#Train Samples	#Test Samples	Total #Samples	Precision (%)	Recall (%)	Precision (%)	Recall (%)
Transmission-tower	4000	1460	5460	80.88	84.01	81.80	85.47
Spacer	2690	466	3156	78.89	86.91	81.89	92.97
Balisor	315	83	398	100.00	100.00	100.00	100.00
Lightning-arrester	2980	456	3436	83.93	89.40	84.91	90.77
PorSTI-W+PorSTI-R	7402	992	8394	91.89	97.05	93.40	97.49
Insulator (polymer)	798	50	848	92.25	95.34	93.33	96.23
Damper-weight	4090	350	4440	77.21	74.98	79.81	81.47
Sag adjuster	1832	332	2164	71.87	86.62	75.43	87.22
Avg.	24116	4180	28296	84.62	89.29	86.36	91.42

Table 1. Performance summary of Jetson TX^2 embedded real time CNN detector

Method	Size of the Evaluation Dataset	Recall (%)	Precision (%)	Avg. Precision (%)
Wu and An	50	86.45	85.61	86.05
Liao and AN	100	91.00	87.00	89.00
Oberweg et al.	375	98.02	32.98	65.52
Jabid	500	94.22	89.56	91.88
Zhao et al.	380	75.02	84.98	80.00
Liu et al.	500	87.55	94.38	90.95
Miao et al.	200	90.00	93.77	91.88
Tao et al.	385	96.62	90.38	93.52
Han et al.	1356	87.38	89.94	88.68
Proposed	990	97.46	93.43	95.47

Table 2. Comparing the proposed CNN-based detector with the most advanced insulator detectors available

Method	Precision@80%Recall	Speed (ms)
EDLines	52.31	78.27
LSD	35.11	415.00
Proposed	90.58	30.20

Table 3. Performance comparison of the most recent technique with the suggested power line identification algorithm

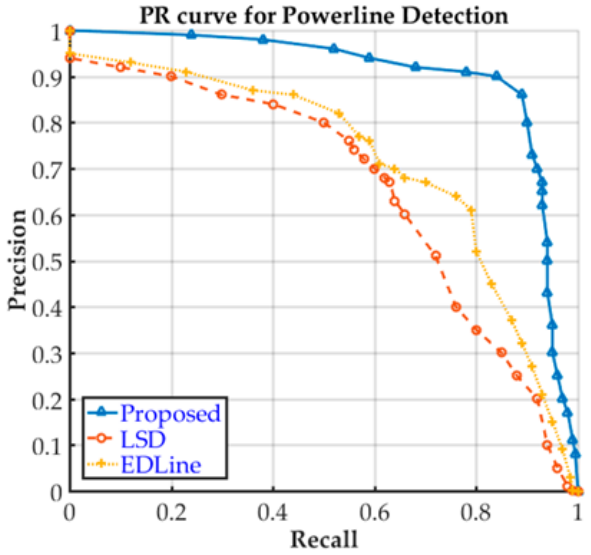

Figure 13. The main efficacy of the suggested power line detection strategy is displayed by the power line detection PR curve

reasons why the CNN-based approach for identifying transmission line component problems is not workable. The results of the defect identification process for the responder's fading, the sag adjuster's rusting, the polymer insulators' crack detection, and the shell breakage faults are displayed in Table 4. The outcomes of the suggested shed detecting technique were contrasted with those of the most recent technology.

Without the need for training, the suggested approach successfully reduces the performance difference between manually constructed feature-based approaches and CNN-based methods. Table 4 further demonstrates that VGG-16, a faster method for the base network, is not only slower than the suggested way but also performs poorly.

With the exception of the split defect analyzer, the overall performance of these defect analyzers suggests that these three flaw detection systems have a lot of room for future advancement. Because segmentation detection techniques rely so largely on edge detection quality, their accuracy is quite low. Noisy edges may produce more false positives due to shadows, obscured objects, deformation of polymer surfaces, varying lighting conditions, and inaccurate cap detection.

	Method	#of Test Samples	Precision (%)	Recall	Processing Time (s)	Training Time and GPU
	ResNet	60	91.00	95.82	0.147	16h on GTX-1080
	VGG-16		41.50	62.90	0.080	
Broken shed	Proposed	75	87.50	93.33	0.066	Not required
Balisor fading	Proposed	75	76.20	100.00	0.101	Not required
Rust in sag adjusters	Proposed	76	70.25	92.33	0.071	Not required
Splits in PolSTI	Proposed	210	38.82	93.77	0.151	Not required

Table 4. Summary of defect detection scheme performance

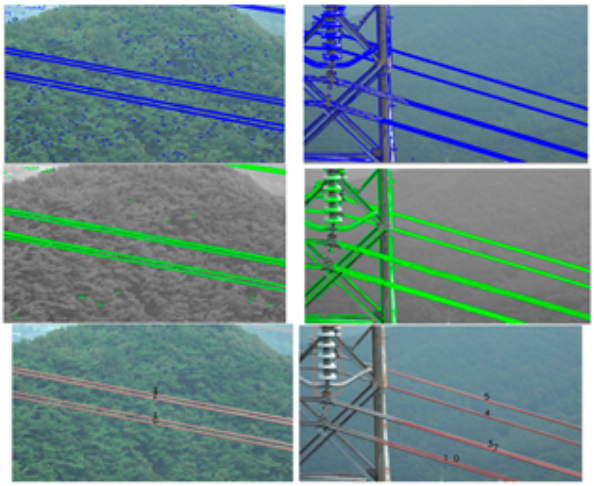

Figure 14. Results of a power cord detection example. Line 1: LSD; Line 2: EDLines; Line 3: Suggested plan

It is advised to record inspection videos between the hours of 8 a.m. and 11 a.m. and 1 p.m. and 5 p.m. on sunny days for optimal results. The lighting isn't particularly harsh or dim right now. You can take films with good visibility at any time on cloudy days. The author advises against taking inspection videos in inclement weather because of the potential for mishaps, even if the inspection drone is made to operate in harsh circumstances including wind, rain, and snow.

6 Conclusion

This article proposes a digital terrain classification and automatic micro terrain extraction method for transmission line engineering based on artificial intelligence enhancement. By combining convolutional neural networks and progressive triangulation algorithms, effective processing of large-scale point cloud data has been achieved, enabling precise extraction and classification of micro terrain. The experimental results show that this method not only significantly improves the accuracy of terrain classification, but also enhances the efficiency of extracting micro terrain details, demonstrating excellent robustness and adaptability in complex terrain environments. In addition, compared with traditional methods, the algorithm proposed in this study has significant advantages in computational efficiency and resource consumption, and can effectively cope with scenarios in transmission line engineering that require high terrain accuracy and detail. This study provides innovative technical means for terrain modeling and analysis in power engineering, with broad application prospects. Meanwhile, future research will further optimize the efficiency of algorithms, explore the adaptability of more types of terrain data, and enhance the scalability and universality of models in practical engineering applications.

References

[1] Shakiba, F. M., Azizi, S. M., Zhou, M., & Abusorrah, A. (2023). Application of machine learning methods in fault detection and classification of power transmission lines: a survey. *Artificial Intelligence Review, 56*(7), 5799-5836.

[2] Xiao, S., Fan, Q., Wu, J., Zhao, C., & Wu, D. (2023, October). Research and practice of extraction technology for ice-cover-prone micro-topography in Guizhou. In *Sixth International Conference on Computer Information Science and Application Technology* (CISAT 2023) (Vol. 12800, pp. 1312-1318). SPIE.

[3] Deng, Y., Jiang, X., Wang, H., Yang, Y., Virk, M. S., Liao, Y., ... & Zhao, M. (2024). Multimodal analysis of saddle micro-terrain prone to wind disasters on overhead transmission lines. *Electric Power Systems Research, 229*, 110143.

[4] Lv, X. L., & Chiang, H. D. (2024). Visual clustering network-based intelligent power lines inspection system. *Engineering Applications of Artificial Intelligence, 129*, 107572.

[5] Zaidi, M. A., & Tariq, F. (2023). Revolutionizing power line inspection: automated data acquisition through autonomous UAVs in simulated environment. *South Florida Journal of Development, 4*(3), 1199-1215.

[6] Lin, S., Wang, X., & Nan, C. (2024). Slope unit-based genetic landform mapping on Tibetan plateau-a terrain unit-based framework for large spatial scale landform classification. *Catena, 236*, 107757.

[7] Rezapour, H., Jamali, S., & Bahmanyar, A. (2023). Review on artificial intelligence-based fault location methods in power distribution networks. *Energies,*

16(12), 4636.

[8] Luo, Y., Yu, X., Yang, D., & Zhou, B. (2023). A survey of intelligent transmission line inspection based on unmanned aerial vehicle. *Artificial Intelligence Review, 56*(1), 173-201.

[9] Najafzadeh, M., Pouladi, J., Daghigh, A., Beiza, J., & Abedinzade, T. (2024). Fault Detection, Classification and Localization Along the Power Grid Line Using Optimized Machine Learning Algorithms. *International Journal of Computational Intelligence Systems, 17*, 49.

[10] Ahmed, M. F., Mohanta, J. C., Sanyal, A., & Yadav, P. S. (2024). Path planning of unmanned aerial systems for visual inspection of power transmission lines and towers. *IETE Journal of Research, 70*(3), 3259-3279.

[11] Kanwal, S., & Jiriwibhakorn, S. (2023). Artificial intelligence based faults identification, classification, and localization techniques in transmission lines-a review. *IEEE Latin America Transactions, 21*(12), 1291-1305.

[12] Shan, G., Li, G., Wang, Y., Xing, C., Zheng, Y., & Yang, Y. (2023). Application and prospect of artificial intelligence methods in signal integrity prediction and optimization of microsystems. *Micromachines, 14*(2), 344.

[13] Li, M., Dai, W., Song, S., Wang, C., & Tao, Y. (2023). Construction of high-precision DEMs for urban plots. *Annals of GIS, 29*(2), 193-203.

[14] Zahraoui, Y., Korõtko, T., Rosin, A., Mekhilef, S., Seyedmahmoudian, M., Stojcevski, A., & Alhamrouni, I. (2024). AI Applications to Enhance Resilience in Power Systems and Microgrids—A Review. *Sustainability, 16*(12), 4959.

[15] Saqib, K. Postmodernism, Social Dynamics, and E-Commerce Evolution. *International Journal for Housing Science and Its Applications, 45*(1), 20-24.

[16] Guo, L., & Sun, Y. Economic Forecasting Analysis of High-Dimensional Multifractal Action Based on Financial Time Series. *International Journal for Housing Science and Its Applications, 45*, 11-19.

[17] Altay, A., & Mirici, İ. H. (2024). Efl Instructors' Implementations of 21st Century Skills in Their Classes. *International Journal for Housing Science and Its Applications, 45*(2), 37-46.

[18] Lal, M. D., & Varadarajan, R. (2023). A review of machine learning approaches in synchrophasor technology. *IEEE Access, 11*, 33520-33541.

[19] Eristi, B., Yamacli, V., & Eristi, H. (2024). A novel microgrid islanding classification algorithm based on combining hybrid feature extraction approach with deep ResNet model. *Electrical Engineering, 106*(1), 145-164.